


# Bilayer graded Al/B<sub>4</sub>C/rice husk ash composite: Wettability behavior, thermo-mechanical, and electrical properties

Amin Bahrami<sup>1,2,\*</sup> , Niloofar Soltani<sup>1,2,\*</sup>, Martin I Pech-Canul<sup>2</sup>, Shaghayegh Soltani<sup>3</sup>, Luis A González<sup>2</sup>, Carlos A Gutiérrez<sup>2</sup>, Joshua Tapp<sup>4</sup>, Angela Möller<sup>4</sup> and Aleksander Gurlo<sup>5</sup>

Journal of Composite Materials  
2018, Vol. 52(27) 3745–3758  
© The Author(s) 2018  
Article reuse guidelines:  
sagepub.com/journals-permissions  
DOI: 10.1177/0021998318769993  
journals.sagepub.com/home/jcm



## Abstract

In this study, wettability behavior of B<sub>4</sub>C substrate as well as B<sub>4</sub>C/crystalline rice husk ash and B<sub>4</sub>C/amorphous rice husk ash substrates with two aluminum alloys were studied. The electrical resistivity, thermal expansion coefficients, and thermal diffusivity of bilayer Al/B<sub>4</sub>C/rice husk ash composite fabricated by one-step pressureless infiltration were measured and the obtained data were systemically analyzed using the Taguchi method and analysis of variance. Boron carbide substrates after addition of amorphous or crystalline rice husk ash display good wettability with molten aluminum alloys. The results show that, electrical resistivity of Al/B<sub>4</sub>C/rice husk ash composites is mainly influenced by initial preform porosity, while the coefficient of thermal expansion of composites is determined by the chemical composition of infiltrated alloys. The measured values for coefficient of thermal expansion ( $10.5 \times 10^{-6}/^{\circ}\text{C}$ ) and electrical resistivity ( $0.60 \times 10^{-5} \Omega\cdot\text{m}$ ) of Al/B<sub>4</sub>C/rice husk ash composites, fabricated according to analysis of variance's optimal conditions are in good agreement with those of the projected values ( $11.02 \times 10^{-6}/^{\circ}\text{C}$  and  $0.65 \times 10^{-5} \Omega\cdot\text{m}$ , respectively). The difference between the corresponding values obtained from verification tests and projected values, for electrical resistivity and coefficient of thermal expansion are less than 5%. Finally, as a material selection approach, the strengths and weaknesses of the composites have been graphed in the form of radar diagrams.

## Keywords

Rice husk ash, pressureless infiltration, wettability, thermo-mechanical analyses, electrical resistivity

## Introduction

To make a lightweight material which possesses properties such as high thermal conductivity, low coefficient of thermal expansion (CTE), and high strength at higher temperatures, using high percentage of ceramics with high strength and low CTE in a metallic matrix would be desirable.<sup>1–4</sup> These types of metal matrix composites (MMCs) have attractive properties for armor applications, multifunctional electronic packaging, and support structures in optical systems.<sup>5–8</sup> Among the different MMCs, Al/B<sub>4</sub>C composites with a high volume fraction of particulate reinforcement are a suitable and versatile option due to outstanding physical properties of B<sub>4</sub>C particles.<sup>9,10</sup> Infiltration of ceramic preforms by liquid metals not only provides a

<sup>1</sup>Instituto de Investigaciones en Materiales, Universidad Nacional Autónoma de México, Ciudad Universitaria, Mexico

<sup>2</sup>Centro de Investigación y de Estudios Avanzados del IPN Unidad Saltillo, Mexico

<sup>3</sup>School of Engineering and Digital Arts, University of Kent, Canterbury, UK

<sup>4</sup>Institute of Inorganic and Analytical Chemistry, Johannes Gutenberg-University Mainz, Germany

<sup>5</sup>Fachgebiet Keramische Werkstoffe, Institut für Werkstoffwissenschaften und – Technologien, Technische Universität Berlin, Germany

\*The first two authors contributed equally to this work.

### Corresponding author:

Amin Bahrami, Circuito Exterior, Ciudad Universitaria, Coyoacán, Ciudad de México 04510, Mexico.

Email: amin.bahrami@iim.unam.mx

constitutive route for the processing of composite materials with high percentage of reinforcement, but also offers the potential to produce graded composite materials by variation of shape, size, and volume fraction of the reinforcement in each layer.<sup>11–14</sup> However, in order to improve the quality of the final composite, understanding the reactive wetting behavior of molten alloys in contact with ceramic substrates at high temperatures is essential. The study of the wetting behavior at elevated temperatures, therefore, constitutes one of the most important scientific aspects of high-temperature liquid phase materials processing.<sup>15</sup>

In the previous study, successful fabrication of bilayer graded Al/B<sub>4</sub>C/MgAl<sub>2</sub>O<sub>4</sub> composite by pressureless infiltration method as well as its promising mechanical properties have been reported.<sup>16</sup> In that study, it was shown that addition of rice husk ash (RHA) as a source of oxygen causes formation of MgAl<sub>2</sub>O<sub>4</sub> phase which improve the mechanical properties of final composite. Amongst the various known biomasses, with abundant and renewable energy sources, RH is not only a potential source of energy, but also a value-added byproduct. RHs contain organic substances and 20% of inorganic material. The main elemental components of RH are C 37.05 wt.%, H 8.80 wt.%, N 11.06 wt.%, Si 9.01 wt.%, and O 35.03 wt.%.<sup>7,17</sup>

In order to evaluate the effect of amorphous rice husk ash (ARHA) and crystalline rice husk ash (CHRA) incorporation on the wettability behavior of B<sub>4</sub>C substrate and physical properties of bilayer Al/B<sub>4</sub>C composite, a two-fold objective has been established for this investigation. First, using the sessile drop method, the wetting behavior of B<sub>4</sub>C substrate by two Al-Si-Mg alloys has been investigated. The study also includes analyzing the effect of incorporating CRHA and ARHA into B<sub>4</sub>C powder-compact substrates. Second, the effect of processing parameters on the physical properties (CTE, electrical resistivity, and thermal diffusivity) of Al/B<sub>4</sub>C/RHA composites has been studied. Also, to determine the variability in the response parameters in an experiment, analysis of variance (ANOVA) has been used. This method provides a means of estimating the percent contribution of each of the parameters tested to the variability in the measured response variable.

## Experimental procedure

Aluminum cubs were cut in the size of 10 × 10 × 10 mm from as-cast aluminum alloys to be melted on B<sub>4</sub>C, B<sub>4</sub>C/CRHA, and B<sub>4</sub>C/ARHA substrates during the sessile drop test. Chemical compositions of both starting alloys used in this study are presented in Table 1. Based on the test parameters, the prepared blocks were placed on the top of loose beds of B<sub>4</sub>C powders and of mixtures of B<sub>4</sub>C/SiO<sub>2</sub> (from RH) powders. The prepared specimen was placed into a horizontal tube furnace, and heated up to the test temperature at a rate of 20°C/min under nitrogen or argon atmosphere (99.999% Ultra High Purity, O<sub>2</sub> < 2 ppm). During the tests, the droplets were photographed to determine the contact angle as a function of temperature and time.

Infiltration tests for composites of Al/B<sub>4</sub>C/RHA were conducted under the conditions shown in Table 2. The effect of various parameters on the physical properties of composite was investigated using the Taguchi method for design of experiments.<sup>18</sup> Infiltration temperature, time, particle size, porosity of preform, SiO<sub>2</sub> crystallinity, and content in the bilayer preform were used as parameters of infiltration process. The fabrication method as well as fabrication conditions have been discussed in detail elsewhere.<sup>16</sup> Table 3 shows L12 Taguchi tables used for this study.

**Table 2.** Parameters and levels tested in this experiment.

Parameter	Level 1	Level 2
B <sub>4</sub> C particle size (μm)	9/130	130/9
Porosity of preform (%)	40/60	60/40
Alloy	Low Mg	High Mg
SiO <sub>2</sub> content (wt.%)	10	5
Time (min)	60	120
Temperature (°C)	1150	1250
SiO <sub>2</sub> crystallinity	Crystalline	Amorphous
Constants	<ul style="list-style-type: none"> <li>• Ar flow rate: 50 cm<sup>3</sup>/min.</li> <li>• Alloy amount: 50g.</li> </ul>	<ul style="list-style-type: none"> <li>• Geometry and size of cuboid preform: for each layer: 20 × 10 × 50 mm.</li> </ul>

**Table 1.** Chemical composition of aluminum alloys used in the experiments (wt.%).

Elements	Si	Mg	Fe	Mn	Zn	Al
Alloy 1 (Low Mg)	13.1	9.2	0.244	0.038	0.066	Base
Alloy 2 (High Mg)	12.7	13.5	0.277	0.038	0.055	Base

**Table 3.** Standard L12 Taguchi table for pressureless infiltration of this study.

Number	Particle size	Porosity	Alloy	SiO <sub>2</sub> %	Time	Temp.	Crystallinity
1	1	1	1	1	1	1	1
2	1	1	1	1	1	2	2
3	1	1	2	2	2	1	1
4	1	2	1	2	2	1	2
5	1	2	2	1	2	2	1
6	1	2	2	2	1	2	2
7	2	1	2	2	1	1	2
8	2	1	2	1	2	2	2
9	2	1	1	2	2	2	1
10	2	2	2	1	1	1	1
11	2	2	1	2	1	2	1
12	2	2	1	1	2	1	1

Cuboid samples with the dimension of  $3 \times 3 \times 2$  mm were cut for thermo-mechanical measurements, while thin plate of  $10 \times 10 \times 1$  mm were used for X-ray powder diffraction (XRD) analyses and electrical resistivity measurement. The XRD tests were performed using Philips –3040 XRD equipment (Cu K $\alpha$  radiation, anode excitation of 40 kV, and current of 30 mA). CTE values were measured by TMA 402 F1/F3 Hyperion<sup>®</sup>, a Thermo-mechanical Analyzer—Vertical Dilatometer. All samples were heated up and cooled down with the rate of 20°C/min under protective atmosphere of high purity nitrogen with the flow rate of 30 cm<sup>3</sup>/min.

Electrical resistivity was measured using four-point probe technique (Lucas Labs S-302 Four Point Probe) on the flat faces of the samples. The measurement was conducted using direct current (DC) to avoid skin effects associated with alternating current (AC) in the matrix and transient polarization phenomena in the ceramic component. The thermal diffusivity ( $\alpha$ ) was measured by the laser flash method on square samples of dimensions  $8 \times 8 \times 1$  mm, using a Netzsch LFA 457 MicroFlash<sup>TM</sup> diffusivity apparatus. Measurements were done from room temperature up to 300°C in an argon atmosphere.

## Results and discussion

### Wettability behavior of B<sub>4</sub>C, B<sub>4</sub>C/ARHA, and B<sub>4</sub>C/CRHA substrates

Figure 1(a) shows the variations in contact angles with temperature and time for the molten Al alloys on B<sub>4</sub>C surfaces at 1200°C. As it can be seen from Figure 1, all the systems show a similar behavior of the contact angle vs. temperature and time over the entire temperature and time range, and the contact angle depends on both the process atmosphere and the type of alloy

(Mg content). The contact angles decreased rapidly in the initial several minutes (considering heating rate of 5°C/min, 20 min) and then approaches a steady value gradually, while the time needed to reach the steady value changes with the altering alloys or atmosphere. The final contact angles reach 51.8° (N<sub>2</sub>, low-Mg alloy), 48.3° (Ar, low-Mg alloy), 45.1° (N<sub>2</sub>, high-Mg alloy), and 40.6° (Ar, high-Mg alloy) after 90 min of heat preservation. These results are in good agreement with the previous studies. Halverson et al.<sup>19</sup> reported that final contact angle of aluminum on B<sub>4</sub>C substrate can reach to 66° in argon atmosphere after 180 min heating at 1200°C. The observed difference between the reported result<sup>19</sup> and experimental result from this study could be related to the presence of Si and Mg elements which reduce the surface tension of aluminum alloys. The lower surface tension of aluminum alloys in contact with B<sub>4</sub>C in argon atmosphere (Figure 1(b)) can be attributed to interface reactions which occur during the contacting time.<sup>20</sup> As it can be seen from Figure 1(b), magnesium content has more effect in reducing the surface tension of aluminum alloys than type of atmosphere.

Many researches have been done to investigate the effects of interface reaction on the wetting behavior of Al/B<sub>4</sub>C, but its wetting mechanism is subject to controversy. Viala et al.<sup>21</sup> and Arslan et al.<sup>22</sup> believe that in Al/B<sub>4</sub>C system, the wetting is only associated with the formation of Al<sub>3</sub>BC, while the formation of AlB<sub>2</sub> and AlB<sub>12</sub> phases has no significant effect on wetting due to the fact that B<sub>4</sub>C particles are generally surrounded by Al<sub>3</sub>BC crystals. This result is in agreement with the work of Fujii et al.<sup>23</sup> who did not detect uniformly distributed  $\alpha$ -AlB<sub>12</sub> and AlB<sub>2</sub> crystals throughout the BN–Al interface. However, Lin et al.<sup>24</sup> and Kharlamov<sup>25</sup> consider that the wettability of B<sub>4</sub>C by pure Al is determined by the formation of

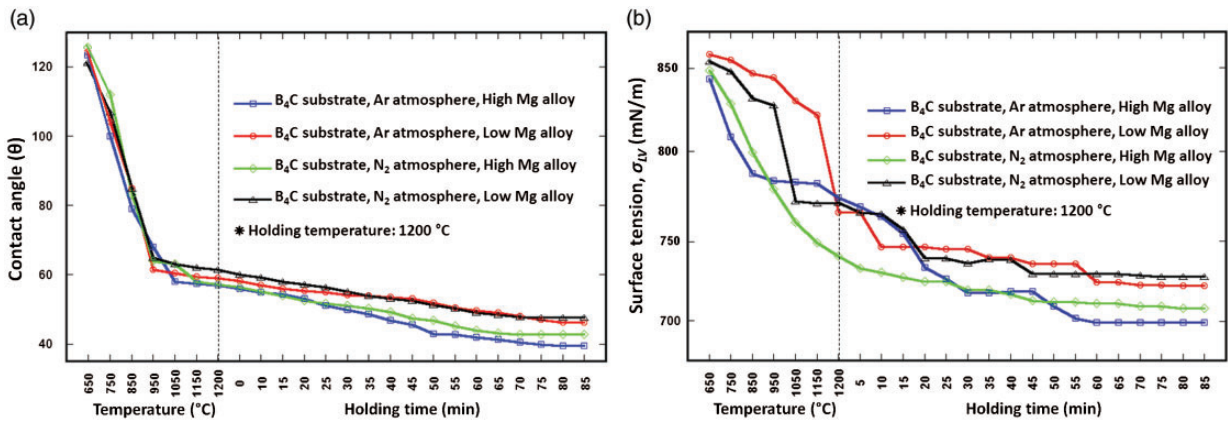


**Figure 1.** Variation of droplet (a) contact angle and (b) surface tension as a function of temperature and time during the isothermal period of 1200 $^{\circ}\text{C}$  in trials performed in argon and nitrogen atmosphere.

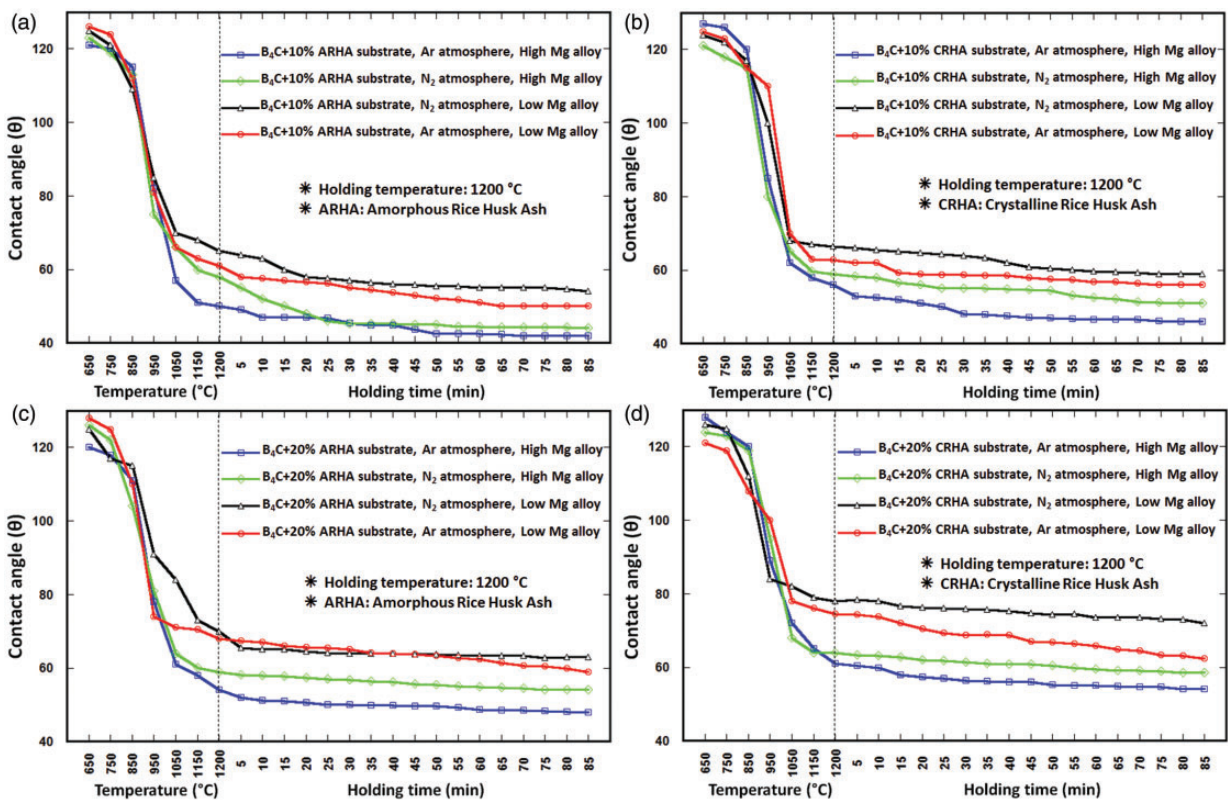


**Figure 2.** Variation of alloy contact angle ( $\theta$ ) as a function of temperature and time during the isothermal periods (1200 $^{\circ}\text{C}$ ) in trials performed with different chemical composition of Al alloy on  $\text{B}_4\text{C}/\text{RHA}$  substrates, (a)  $\text{B}_4\text{C}/10\text{wt.}\% \text{ ARHA}$ , (b)  $\text{B}_4\text{C}/10\text{wt.}\% \text{ CRHA}$ , (c)  $\text{B}_4\text{C}/20\text{wt.}\% \text{ ARHA}$ , and (d)  $\text{B}_4\text{C}/20\text{wt.}\% \text{ CRHA}$  tested in argon and nitrogen atmospheres.

different reaction products, where the  $\text{Al}_3\text{BC}$  phase makes a considerable contribution to the wettability.

Figure 2 shows the changes in contact angle of two different aluminum alloys on different substrates of  $\text{B}_4\text{C}/\text{RHA}$  substrates with different weight percentage of RHA. As it can be seen from the mentioned figures, increasing the amount of RHA in all the conditions

causes an augmentation in molten drop contact angle. This increment will be intensified when CRHA is incorporated into the substrate. As it can be seen from Figure 2, incorporation of crystalline silica to  $\text{B}_4\text{C}$  powders increases the contact angle of aluminum alloys on  $\text{B}_4\text{C}/\text{RHA}$  but does not make the substrate non-wettable by neither of the aluminum alloys.



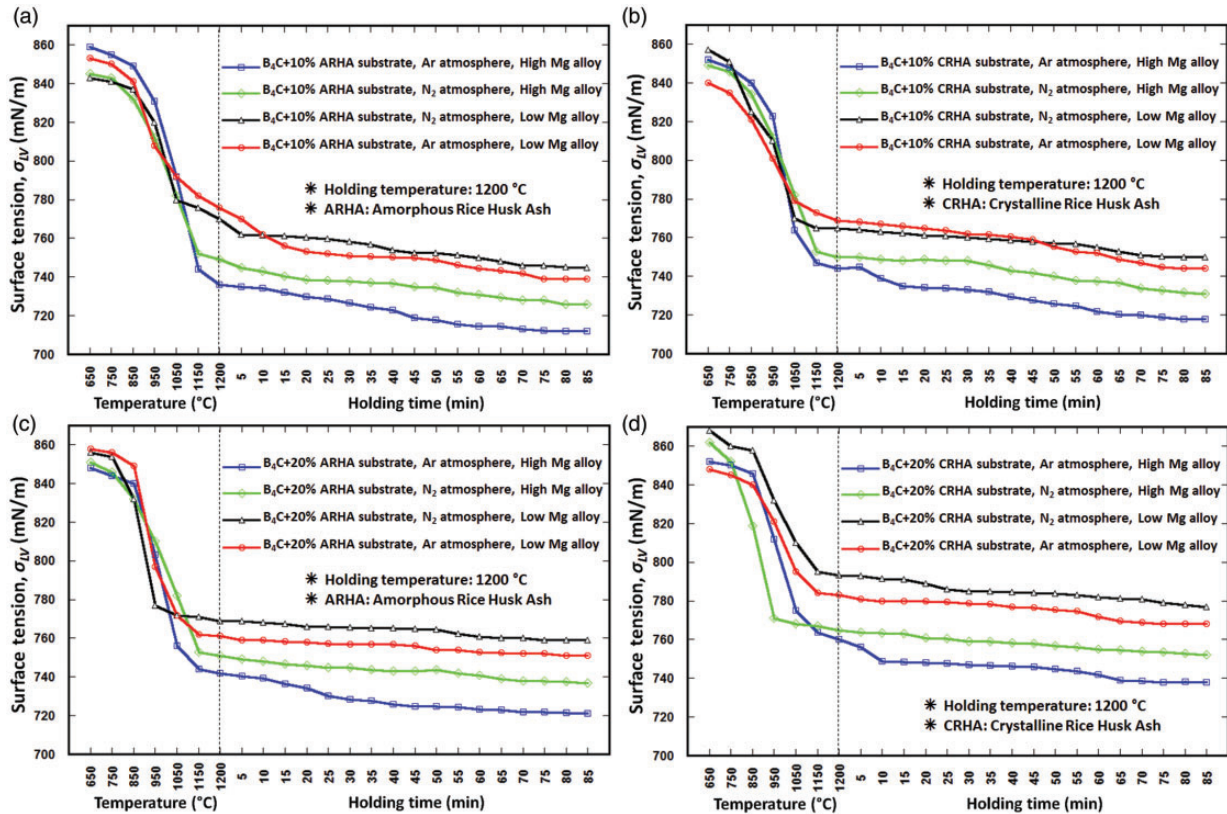


**Figure 3.** Variation of alloy surface tension ( $\sigma_{lv}$ ) as a function of temperature and time during the isothermal periods (1200°C) in trials performed with different chemical composition of Al alloy on  $B_4C/RHA$  substrates, (a)  $B_4C/10\text{wt.}\%$  ARHA, (b)  $B_4C/10\text{wt.}\%$  CRHA, (c)  $B_4C/20\text{wt.}\%$  ARHA, and (d)  $B_4C/20\text{wt.}\%$  CRHA tested in argon and nitrogen atmospheres.

The minimum and maximum contact angles are belonged to the high Mg alloy on  $B_4C/10\text{wt.}\%$  ARHA and low Mg alloy on  $B_4C/20\text{wt.}\%$  CRHA with the value of  $42^\circ$  and  $73^\circ$ , respectively.

According to Young–Dupre’s equation,<sup>26</sup> the contact angle,  $\theta$ , can be decreased by increasing the surface energy of the solid,  $\gamma_{sl}$ , decreasing the solid/liquid interfacial energy,  $\gamma_{sl}$ , or by decreasing the surface tension of the liquid,  $\gamma_{lv}$ . During heating, the silicon is believed to diffuse from the  $B_4C/SiO_2$  substrates into the molten Al drop. The silicon concentration will therefore increase in the contacting surface of Al drop with substrate because of the silicon diffusion. As the wetting test goes on, the silicon can reduce the surface tension of molten aluminum, and thus  $\gamma_{lv}$  is decreased<sup>27</sup> by the adsorption of silicon on the interface and surface of the liquid. On the other hand, the solid/liquid interfacial energy,  $\gamma_{sl}$ , can also be decreased due to the enrichment of silicon on the interface. As a result, the contact angle,  $\theta$ , will be decreased.<sup>28</sup> Figure 4 shows the cross section of the high Mg alloys in contact with  $B_4C/20\text{wt.}\%$  ARHA. As it can be seen, the concentration of Si is higher in the surface of alloy which is in contact with ceramic substrate. It can be attributed to the free

Si which can be released during the reaction of RHA particles with molten aluminum during the process.

### Physical properties of Al/ $B_4C/MgAl_2O_4$ composites

In this study RHA was used as an oxygen source to form in situ  $MgAl_2O_4$  phase in reaction with Al-Mg-Si alloy during infiltration process.<sup>7,17</sup> Microstructure evaluation and phase characterization as well as possible chemical reactions between amorphous and crystalline silica derived from RH and  $B_4C$  with aluminum alloys have been discussed in our previous works extensively.<sup>16,29</sup> Figure 5 shows the abrupt changes in the microstructure of bilayer Al/ $B_4C/RHA$  composite fabricated according to L7 test condition. It can be seen, in the layer with smaller  $B_4C$  particles size, more ceramic phases have been formed which is due to the high surface area of the fine  $B_4C$  particles which causes higher reaction of Al with  $B_4C$  than in the layer which contains  $B_4C$  of large size.  $MgAl_2O_4$ ,  $Al_4C_3$ ,  $Al_3BC$ ,  $Al_8B_4C_7$ , and  $AlB_2$  are the main ceramic phases that were detected by XRD in the prepared composites.<sup>16</sup> It has been reported that the phase composition of Al/ $B_4C$  composites is highly depended on

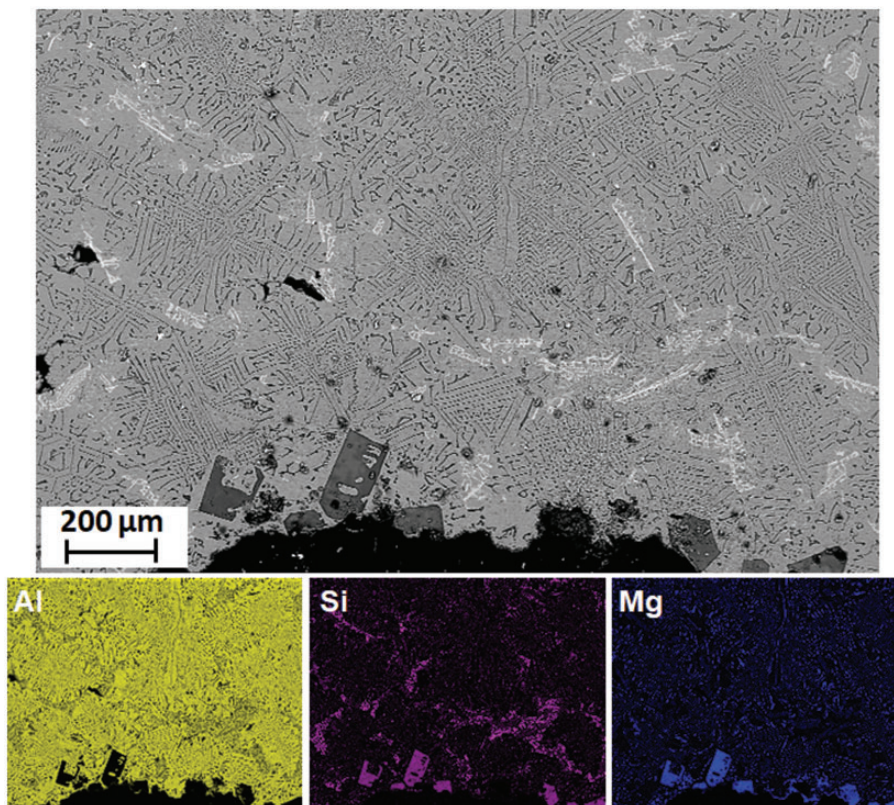


**Figure 4.** BSE micrographs of the cross section of the molten High Mg aluminum alloy droplets on  $B_4C/20$  wt.% ARHA at  $1200^\circ C$  for 90 min.

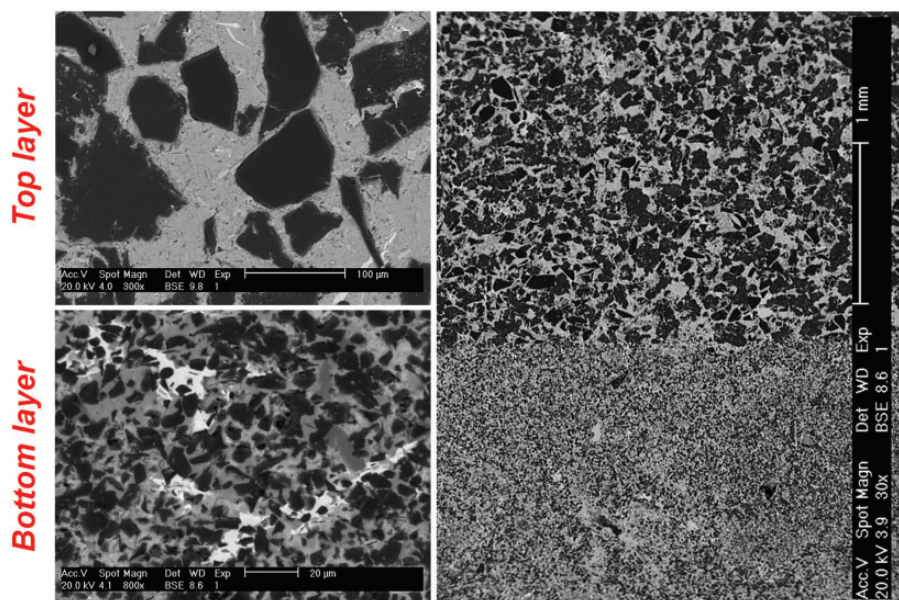


**Figure 5.** SEM micrograph of both layers of fabricated composite according to configuration L7.



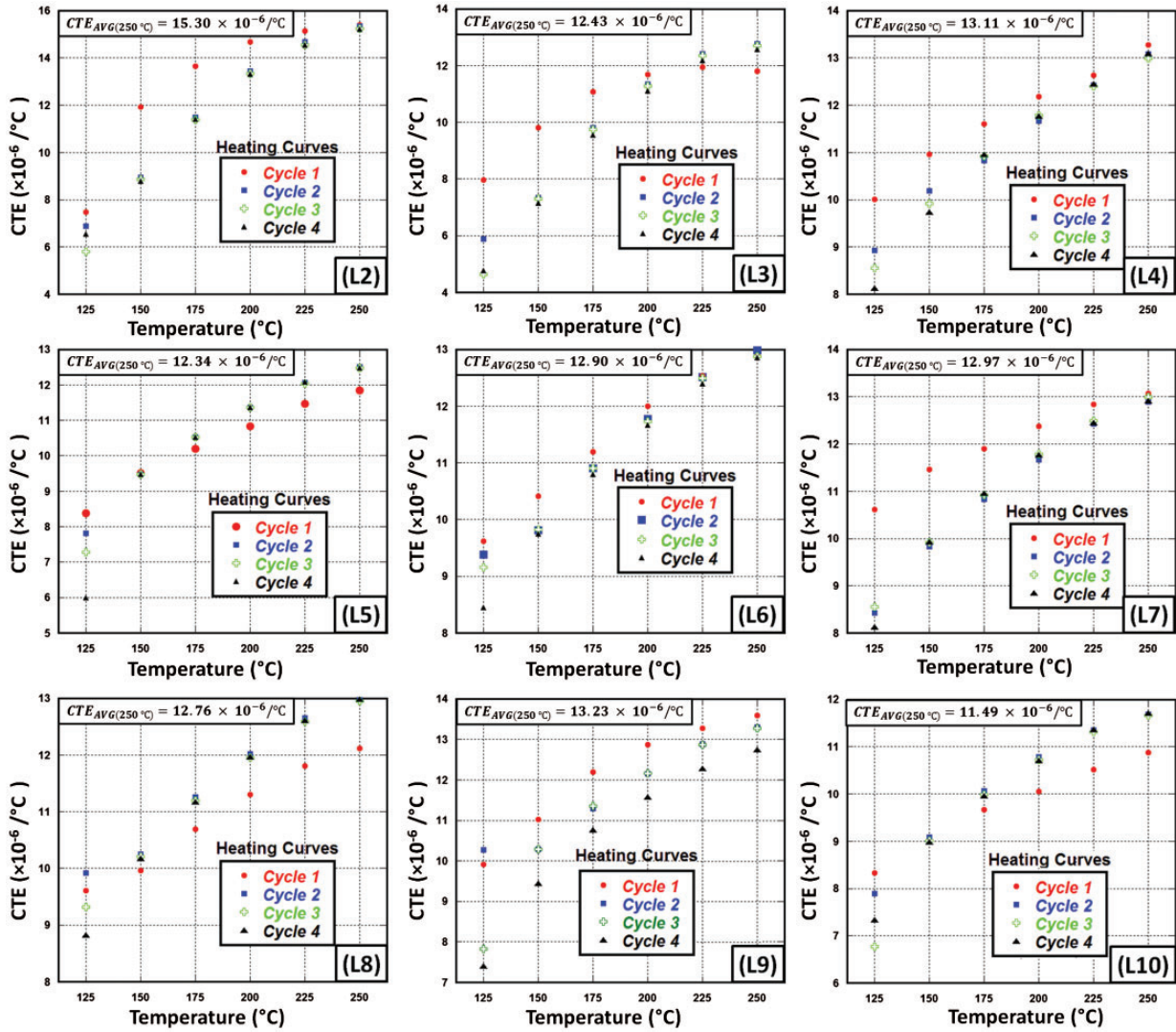


**Figure 6.** CTE values obtained during the four cycles of heating and cooling between 25°C and 250°C on Al/B<sub>4</sub>C/MgAl<sub>2</sub>O<sub>4</sub> composites.  
 CTE: coefficient of thermal expansion.

**Table 4.** CTE values calculated from heating curves of thermal strain response curve of Al/B<sub>4</sub>C/MgAl<sub>2</sub>O<sub>4</sub> composites, obtained during the four cycles of heating and cooling.

Composites	$\epsilon^p$	$\epsilon^c$	$\Delta\epsilon^t (10^{-3})$	CTE ( $10^{-6}/^\circ\text{C}$ )
L2	0.0007634	0.002212	1.594	15.30
L3	0.0003353	0.001946	1.106	12.43
L4	0.0003829	0.001975	1.327	13.11
L5	0.0003075	0.001838	1.097	12.34
L6	0.0005228	0.002188	1.133	12.90
L7	0.0005652	0.002207	1.155	12.97
L8	0.0004024	0.002185	1.131	12.76
L9	0.0007351	0.002426	1.350	13.23
L10	0.0002732	0.001761	1.039	11.49

CTE: coefficient of thermal expansion.

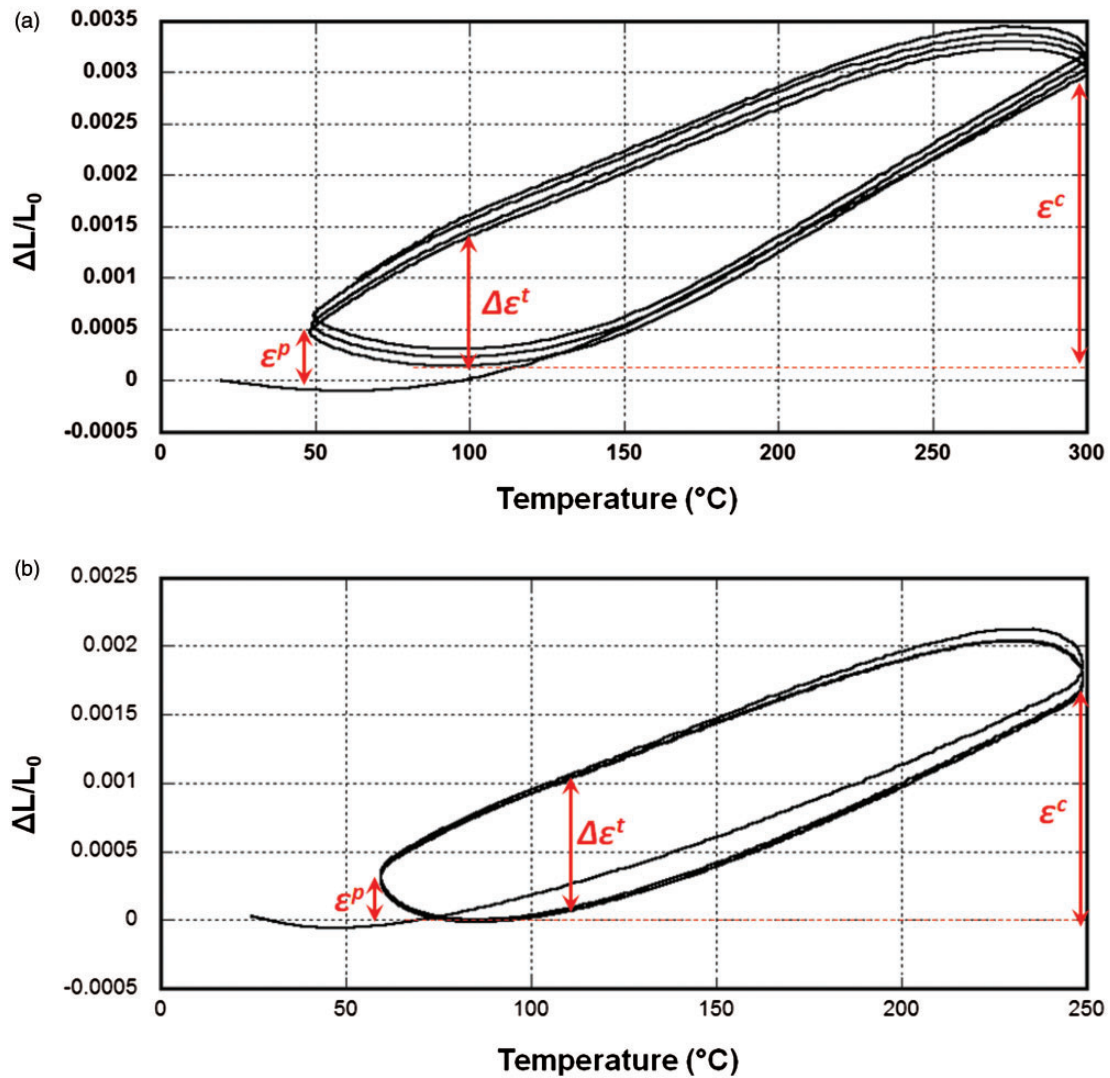


**Figure 7.** Thermal strain response curves recorded during the four cycles between 25 and 250 and 300°C on (a) L2, and (b) L10-Al/ $B_4C/MgAl_2O_4$  bilayer composite.

**Table 5.** Pooled ANOVA table for minimum CTE value of Al/ $B_4C/MgAl_2O_4$  composite.

Column	Factors	Sum of squares	Variance	Contribution percentage
1	$B_4C$ particle size	0.81	0.81	7
2	Porosity of preform	1.71	1.71	15
3	Alloy	3.91	3.91	35
4	$SiO_2$ content	0.004	Pooled	—
5	Time	0.34	0.34	3
6	Temperature	1.44	1.44	13
7	$SiO_2$ crystallinity	2.38	2.38	21
Error		0.65		6
Total		10.94		

CTE: coefficient of thermal expansion; ANOVA: analysis of variance.



**Table 6.** Optimum process parameters for minimum CTE value of Al/B<sub>4</sub>C/MgAl<sub>2</sub>O<sub>4</sub> composite.

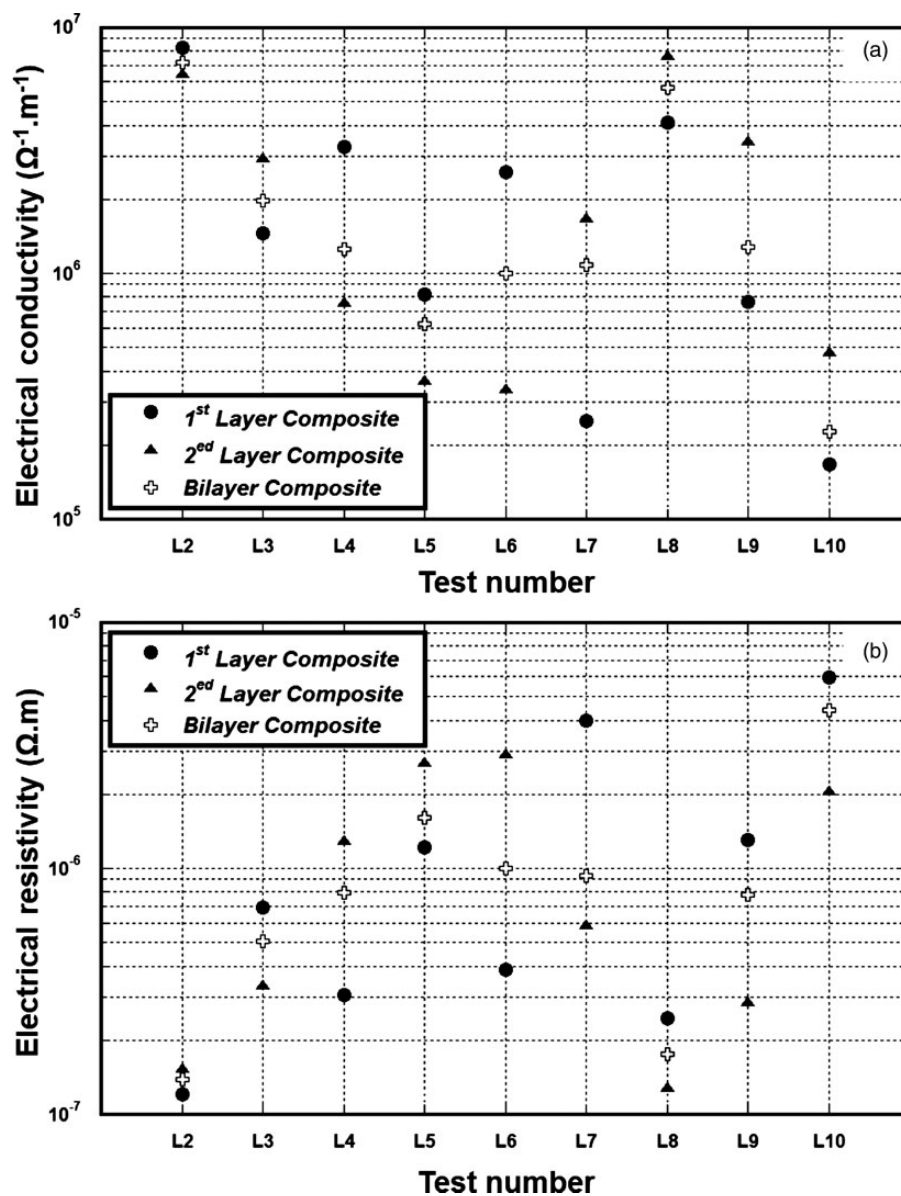
Parameters	Proposed levels
B <sub>4</sub> C particle size (μm)	130/9
Porosity of preform (%)	60/40
Alloy	Low Mg
SiO <sub>2</sub> content (wt.%)	10
Time (min)	60
Temperature (°C)	1150
SiO <sub>2</sub> crystallinity	Crystal

CTE: coefficient of thermal expansion.

the following factors: (a) thermal or chemical treatment of boron carbide before metal infiltration, (b) the time and temperature of composite densification, and (c) the heat treatment processes after composite fabrication.<sup>30,31</sup>

### Thermo-mechanical analyses

CTE values of all starting materials including amorphous and crystalline SiO<sub>2</sub>, Al-13Si-14Mg, and Al-13Si-9Mg were reported elsewhere.<sup>32</sup> Figure 6 shows CTE values obtained from thermal strain response curves of all fabricated Al/B<sub>4</sub>C/RHA composites. As it can be seen L10 composite has the lowest CTE values

**Figure 8.** Electrical (a) conductivity and, (b) resistivity of monolayer and bilayer Al/B<sub>4</sub>C/MgAl<sub>2</sub>O<sub>4</sub> fabricated composites.

( $11.49 \times 10^{-6}/^{\circ}\text{C}$ ) among others followed by L5 composite ( $12.34 \times 10^{-6}/^{\circ}\text{C}$ ). The thermal response results ( $\epsilon^p$ ,  $\epsilon^c$ , and  $\Delta\epsilon^f$ ) of all Al/B<sub>4</sub>C/RHA fabricated composites from the heating of the first cycle to the cooling of the fourth cycle are shown in Table 3. As it can be seen from Figure 6 and Table 4 lowest factors are belonged to the Al/B<sub>4</sub>C/RHA composites with lowest CTE values. In comparison to values obtained for Al/SiC/RHA composite,<sup>14</sup> although CTE values of Al/SiC/RHA composites are less than that of Al/B<sub>4</sub>C/RHA composites, the latter has higher  $\Delta\epsilon^f$  values.

Figure 7 shows thermal strain response curves recorded during the four cycles between 25 and 250 and 300°C on L2 and L10-Al/B<sub>4</sub>C/RHA bilayer composite. The thermal expansion response of the composite appears in a hysteresis loop. By increasing the temperature, the matrix becomes soft and the thermal stress induced by thermal mismatch between ceramic particles and aluminum thus causes the plastic flow of the matrix.

Essentially this response should be considered to be an intrinsic expansion/contraction response of composite. During cooling stage, with the further decrease of temperature, thermal stress is built up on already stressed sample. When the sample is in its lowest temperature for a several minutes, initially a slightly tumbled thermal expansion response can be seen. Then, by increasing the temperature, the composite starts contracting. It can be attributed to the thermal stress within matrix that has just reached a level higher than the yield strength of the aluminum during the short isothermal at highest temperature, causing the plastic flow of matrix.<sup>33</sup>

Results of the pooled ANOVA for the CTE values of Al/B<sub>4</sub>C/RHA are shown in Table 5. Table 5 indicates that, at the levels studied, the parameter that affects the CTE values of the composites most significantly is chemical composition of alloy. Its relative contribution to the variance in composite CTE is 35%. SiO<sub>2</sub>

crystallinity process also has a significant effect on CTE value of the composite, contributing 21% of the variance.

Considering experiment parameters and levels designed for this study, the minimum CTE value can be obtained by using the process parameters, tabulated in Table 6. When using these process parameters, the projected CTE value is  $11.02 \pm 0.8 \times 10^{-6}/^{\circ}\text{C}$ .

According to the optimum parameters proposed by ANOVA for minimum CTE value, the verification test has been done. The measured CTE was  $10.5 \pm 0.7 \times 10^{-6}/^{\circ}\text{C}$ . This result is in good agreement with the projected values ( $11.02 \pm 0.8 \times 10^{-6}/^{\circ}\text{C}$ ).

## Electrical resistivity

Electrical resistivity of starting alloys used in this study has been measured and reported in previous work,<sup>14</sup> indicating that alloying causes an increase in electrical resistivity of pure aluminum ( $3.05 \times 10^{-8} \Omega\cdot\text{m}$ ) to  $3.7 \times 10^{-8} \Omega\cdot\text{m}$  for Al-13Si-9Mg and  $4.05 \times 10^{-8} \Omega\cdot\text{m}$  for Al-13Si-14Mg. This outcome can be attributed to two main reasons: (a) to the incorporation of metal

**Table 8.** Optimum process parameters for maximum electrical resistivity of Al/B<sub>4</sub>C/MgAl<sub>2</sub>O<sub>4</sub> composite.

Parameters	Proposed levels
B <sub>4</sub> C particle size (μm)	130/9
Porosity of preform (%)	60/40
Alloy	Low Mg
SiO <sub>2</sub> content (wt.%)	5
Time (min)	60
Temperature (°C)	1150
SiO <sub>2</sub> crystallinity	Crystal

**Table 7.** Pooled ANOVA table for maximum electrical resistivity of Al/B<sub>4</sub>C/MgAl<sub>2</sub>O<sub>4</sub> composite.

Column	Factors	Sum of squares	Variance	Contribution percentage
1	B <sub>4</sub> C particle size	2.68E+11	Pooled	–
2	Porosity of preform	1.58E+13	1.58E+13	31
3	Alloy	4.39E+12	4.39E+12	8
4	SiO <sub>2</sub> content	9.93E+12	9.93E+12	19
5	Time	1.01E+11	Pooled	–
6	Temperature	9.06E+12	9.06E+12	17
7	SiO <sub>2</sub> crystallinity	1.09E+13	1.09E+13	21
Error		2E+12		4
Total		5.04E+13		

ANOVA: analysis of variance.

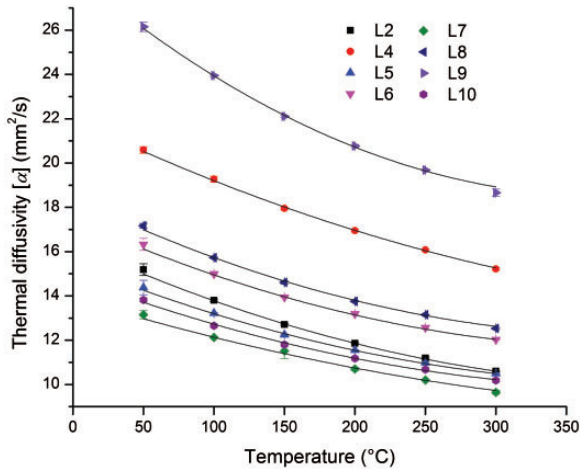


**Figure 9.** Thermal diffusivity of Al/B<sub>4</sub>C/MgAl<sub>2</sub>O<sub>4</sub> bilayer fabricated composite at different temperatures.

atoms into the same crystal lattice, i.e. silicon atoms in the structure of  $\alpha$ -aluminum, hence, a mixed crystal is formed. In this new distorted structure, the electrons find difficulty in moving from atom to atom. Thus, the resistance of the alloy becomes greater. (b) Like in the case for CTE value it can be due to the formation of Mg<sub>2</sub>Si, which has higher electrical resistivity than pure aluminum.

Figure 8 shows the electrical resistivity and conductivity of all monolayer and bilayer Al/B<sub>4</sub>C/RHA fabricated composites. Among all Al/B<sub>4</sub>C/RHA bilayer fabricated composites, highest electrical resistivity ( $4.39 \times 10^{-6} \Omega.m$ ) and lowest electrical conductivity ( $2.28 \times 10^5 \Omega^{-1}.m^{-1}$ ) are belonged to L10 composite. The factors that make L10-Al/B<sub>4</sub>C/RHA bilayer composite the sample with highest electrical resistivity value could be low temperature and short time of infiltration procedure. Those factors prevent reaction of B<sub>4</sub>C with

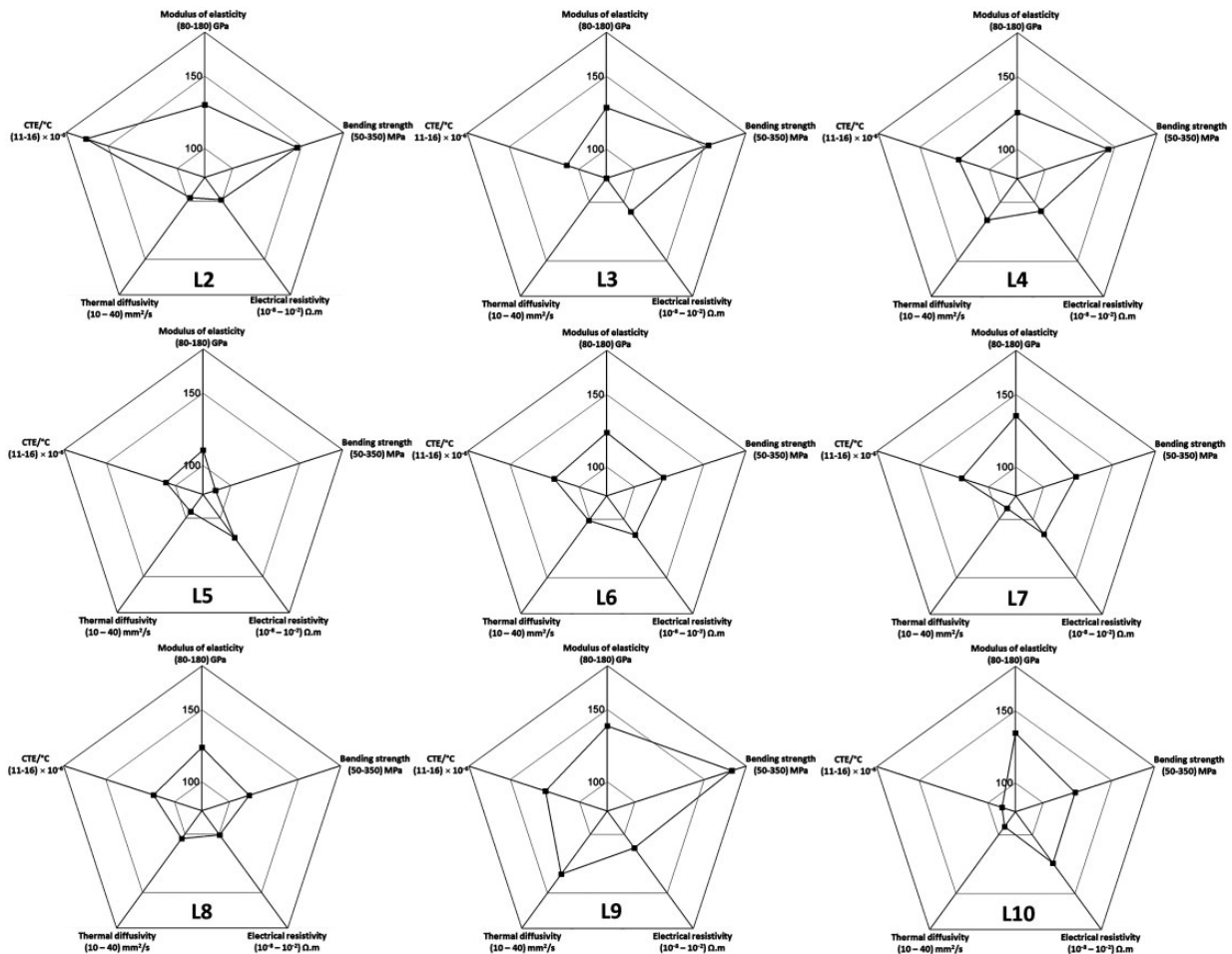


**Figure 10.** Radar graphs for all fabricated bilayer Al/B<sub>4</sub>C/MgAl<sub>2</sub>O<sub>4</sub> composites.



aluminum to form secondary phases such as  $\text{Al}_3\text{BC}$  and  $\text{Al}_8\text{B}_4\text{C}_7$  which their presence were confirmed by XRD patterns of Al/B<sub>4</sub>C/RHA composites.<sup>16</sup> These phases have electrical resistivity less than B<sub>4</sub>C and consequently reduce the electrical resistivity of Al/B<sub>4</sub>C/RHA composites. Therefore, the less reaction of B<sub>4</sub>C with matrix, the more electrical resistivity of Al/B<sub>4</sub>C/RHA.

Results of the pooled ANOVA for electrical resistivity of Al/B<sub>4</sub>C/RHA graded composite are shown in Table 7. It can be concluded from Table 7 that, at the levels studied, the parameter that affects the electrical resistivity of graded composites most significantly is preform porosity followed by SiO<sub>2</sub> crystallinity. Their relative contribution to the variance in the electrical conductivity values are 31% and 21%, respectively. Preform porosity will define the amount of ceramic phases in the composite, therefore it is easy to visualize that by increasing the porosity of each layer electrical resistivity will decrease.

The minimum electrical resistivity can be obtained by using the processing parameters, shown in Table 8. When using these process parameters, the projected electrical resistivity is  $0.65 \times 10^{-5} \pm 0.4 \times 10^{-6} \Omega \cdot \text{m}$ .

The verification test has been done according to the optimum parameters proposed by ANOVA for minimum electrical conductivity. The measured electrical conductivity was  $0.60 \times 10^{-5} \pm 0.6 \times 10^{-5} \Omega \cdot \text{m}$ . This result is in good agreement with the projected values ( $0.65 \times 10^{-5} \pm 0.4 \times 10^{-6} \Omega \cdot \text{m}$ ).

### Thermal diffusivity

As it was reported before, the thermal diffusivity of the starting alloys changes from 97.3 mm<sup>2</sup>/s for pure aluminum to 36.2 mm<sup>2</sup>/s and 25.6 mm<sup>2</sup>/s for Al-13Si-9Mg alloy and Al-13Si-14Mg alloy, respectively, due to the formation of a distorted structure of aluminum after addition of alloying elements of Si and Mg.<sup>14</sup>

Figure 9 shows thermal diffusivity of all fabricated Al/B<sub>4</sub>C/RHA composite. As it can be seen, L9 and L4 samples have highest thermal diffusivity in comparison with other composites. Considering Tables 1 and 2, the common factors between these two configurations are use of Al-13Si-9Mg alloy as a matrix which has higher thermal diffusivity than Al-13Si-14Mg alloy. Also, a low percentage of SiO<sub>2</sub> is associated with a reduced product formation. Except L9 and L4 configurations, the rest almost have the close range thermal diffusivity values. However, L5, L10, and L7 with lowest thermal diffusivity values are fabricated using Al-13Si-14Mg alloy. Therefore, it can be concluded from the results presented for the Al/B<sub>4</sub>C/RHA composites that chemical composition of matrix alloy governs the thermal properties of composite, despite all the

fabricated composites consist of a high percentage of ceramic particles.

As a material selection approach, according to the presented results in this study and previous work,<sup>16</sup> the strengths and weaknesses of the composites have been graphed in the form of radar diagrams in Figure 10. These graphs summarize all physical and mechanical properties of fabricated Al/B<sub>4</sub>C/RHA composites, specifically, the bending strength, modulus of elasticity, electrical resistivity, CTE, and thermal diffusivity, in the one graph and make the materials selection easier and more applicable.

### Conclusions

Based on the above discussed results within the framework of the conducted experiments and within the parameters and levels defined for this project, the following conclusions can be drawn:

1. The reaction products of aluminum with boron carbide particles govern the wettability behavior of B<sub>4</sub>C substrates. The formation of the B-rich phases improves the wettability of B<sub>4</sub>C by aluminum alloys.
2. Addition of ARHA or CRHA to boron carbide substrates does not make the system non-wettable in contact to both aluminum alloys used in this study. The maximum obtained contact angle and surface tension of molten metal in contact with B<sub>4</sub>C/RHA are 73° and 780 mN/m, respectively which are indicative of a wettable system.
3. Among all the processing parameters considered in the study for preparation of Al/B<sub>4</sub>C/RHA composites, chemical composition of alloys has the most significant effect on CTE value, with a contribution percentage of 35%.
4. The electrical resistivity of the composites is mostly affected by the initial preform porosity, with a contribution percentage of 31%, which defines the amount of metallic or ceramic phase in the final composition of the composite.
5. The measured values for CTE ( $10.5 \times 10^{-6}/^\circ\text{C}$ ) and electrical resistivity ( $0.64 \times 10^{-5} \Omega \cdot \text{m}$ ) of Al/B<sub>4</sub>C/RHA composites, fabricated according to ANOVA's optimal conditions are in good agreement with those of the projected values. The difference between the corresponding values obtained from verification tests and projected values, for electrical resistivity and CTE are less than 5%.

### Acknowledgment

Amin Bahrami and Niloofar Soltani gratefully acknowledge PAPIIT-DGAPA for granting a postdoctoral scholarship in Material Research Institute of National Autonomous

University of Mexico (IIM-UNAM), also, CONACYT (National Council of Science and Technology, in Mexico) for granting a doctoral scholarship. The authors are also thankful to CINVESTAV-Salttillo for support in the research activities in the field of advanced materials. AM acknowledges the Carl-Zeiss-Stiftung for support.

### Declaration of Conflicting Interests

The author(s) declared no potential conflicts of interest with respect to the research, authorship, and/or publication of this article.

### Funding

The author(s) disclosed receipt of the following financial support for the research, authorship and/or publication of this article: Angela Möller acknowledges the Carl-Zeiss-Stiftung for support.

### ORCID iD

Amin Bahrami  <http://orcid.org/0000-0001-8851-7351>

### References

- Han Q, Geng Y, Setchi R, et al. Macro and nanoscale wear behaviour of Al-Al<sub>2</sub>O<sub>3</sub> nanocomposites fabricated by selective laser melting. *Compos Part B Eng* 2017; 127: 26–35.
- Hosseini Monazzah A, Pouraliakbar H, Bagheri R, et al. Al-Mg-Si/SiC laminated composites: fabrication, architectural characteristics, toughness, damage tolerance, fracture mechanisms. *Compos Part B Eng* 2017; 125: 49–70.
- Soltani N, Sadrnezhad SK and Bahrami A. Manufacturing wear-resistant 10Ce-TZP/Al<sub>2</sub>O<sub>3</sub> nanoparticle aluminum composite by powder metallurgy processing. *Mater Manuf Process* 2014; 29: 1237–1244.
- Soltani N, Bahrami A, Moghimi FM, et al. The simultaneous effect of extrusion and T6 treatment on the mechanical properties of Al-15wt.%Mg<sub>2</sub>Si composite. *HTM J Heat Treat Mater* 2012; 67: 378–385.
- Zweben C. Advances in composite materials for thermal management in electronic packaging. *JOM* 1998; 50: 47–51.
- Zweben C. Metal-matrix composites for electronic packaging. *JOM* 1992; 44: 15–23.
- Bahrami A, Soltani N, Pech-Canul MI, et al. Development of metal-matrix composites from industrial/agricultural waste materials and their derivatives. *Crit Rev Environ Sci Technol* 2016; 46: 143–208.
- Che Z, Wang Q, Wang L, et al. Interfacial structure evolution of Ti-coated diamond particle reinforced Al matrix composite produced by gas pressure infiltration. *Compos Part B Eng* 2017; 113: 285–290.
- Alizadeh M, Paydar MH and Sharifian Jazi F. Structural evaluation and mechanical properties of nanostructured Al/B<sub>4</sub>C composite fabricated by ARB process. *Compos Part B Eng* 2013; 44: 339–343.
- Karabulut Ş, Gökmen U and Çinicı H. Study on the mechanical and drilling properties of AA7039 composites reinforced with Al<sub>2</sub>O<sub>3</sub>/B<sub>4</sub>C/SiC particles. *Compos Part B Eng* 2016; 93: 43–55.
- Narciso J, Molina JM, Rodríguez A, et al. Effects of infiltration pressure on mechanical properties of Al-12Si/graphite composites for piston engines. *Compos Part B Eng* 2016; 91: 441–447.
- Soltani N, Soltani S, Bahrami A, et al. Electrical and thermomechanical properties of CVI- Si<sub>3</sub>N<sub>4</sub> porous rice husk ash infiltrated by Al-Mg-Si alloys. *J Alloys Compd* 2017; 696: 856–868.
- Dorri Moghadam A, Omrani E, Menezes PL, et al. Mechanical and tribological properties of self-lubricating metal matrix nanocomposites reinforced by carbon nanotubes (CNTs) and graphene – a review. *Compos Part B Eng* 2015; 77: 402–420.
- Bahrami A, Pech-Canul MI, Gutierrez CA, et al. Effect of rice-husk ash on properties of laminated and functionally graded Al/SiC composites by one-step pressureless infiltration. *J Alloys Compd* 2015; 644: 256–266.
- Sobczak N, Singh M and Asthana R. High-temperature wettability measurements in metal/ceramic systems – some methodological issues. *Curr Opin Solid State Mater Sci* 2005; 9: 241–253.
- Bahrami A, Pech-Canul MI, Soltani N, et al. Tailoring microstructure and properties of bilayer-graded Al/B<sub>4</sub>C/MgAl<sub>2</sub>O<sub>4</sub> composites by single-stage pressureless infiltration. *J Alloys Compd* 2017; 694: 408–418.
- Soltani N, Bahrami A, Pech-Canul MI, et al. Review on the physicochemical treatments of rice husk for production of advanced materials. *Chem Eng J* 2015; 264: 899–935.
- Roy RK. *A primer on the Taguchi method*. Dearborn, Michigan, USA: Society of Manufacturing Engineers, 2010.
- Halverson DC, Pyzik AJ and Aksay IA. *Boron-carbide-aluminum and boron-carbide-reactive metal cermets*. Google Patents, 1986.
- Oh SY, Cornie JA and Russell KC. Wetting of ceramic particulates with liquid aluminum alloys: part II. Study of wettability. *MTA* 20: 533–541.
- Viala J, Bouix J, Gonzalez G, et al. Chemical reactivity of aluminium with boron carbide. *J Mater Sci* 1997; 32: 4559–4573.
- Arslan G, Kara F and Turan S. Quantitative X-ray diffraction analysis of reactive infiltrated boron carbide-aluminium composites. *J Eur Ceram Soc* 2003; 23: 1243–1255.
- Fujii H, Nakae H and Okada K. Interfacial reaction wetting in the boron nitride/molten aluminum system. *Acta Metall Mater* 1993; 41: 2963–2971.
- Lin Q, Shen P, Qiu F, et al. Wetting of polycrystalline B<sub>4</sub>C by molten Al at 1173–1473K. *Scr Mater* 2009; 60: 960–963.
- Kharlamov AI. Wetting of hot-pressed aluminum borides and borocarbides by molten aluminum and copper. *Powder Metall Metal Ceram* 2001; 40: 65–70.
- Young T. An essay on the cohesion of fluids. *Philos Trans R Soc Lond* 1805; 95: 65–87.

27. Mouradoff L, Tristant P, Desmaison J, et al. Interaction between liquid aluminium and non-oxide ceramics (AlN, Si<sub>3</sub>N<sub>4</sub>, SiC). *Key Eng Mater* 1995; 113: 177–188.
28. Bahrami A, Pech-Canul MI, Gutiérrez CA, et al. Wetting and reaction characteristics of crystalline and amorphous SiO<sub>2</sub> derived rice-husk ash and SiO<sub>2</sub>/SiC substrates with Al–Si–Mg alloys. *Appl Surf Sci* 2015; 357: 1104–1113.
29. Bahrami A, Pech-Canul MI, Gutiérrez CA, et al. Wetting and reaction characteristics of crystalline and amorphous SiO<sub>2</sub> derived rice-husk ash and SiO<sub>2</sub>/SiC substrates with Al–Si–Mg alloys. *Appl Surf Sci* 2015; 357: 1104–1113.
30. Viala JC, Bouix J, Gonzalez G, et al. Chemical reactivity of aluminium with boron carbide. *J Mater Sci* 1997; 32: 4559–4573.
31. Pyzik AJ and Beaman DR. Al-B-C phase development and effects on mechanical properties of B<sub>4</sub>C/Al-derived composites. *J Am Ceram Soc* 1995; 78: 305–312.
32. Bahrami A, Soltani N, Soltani S, et al. Mechanical, thermal and electrical properties of monolayer and bilayer graded Al/SiC/rice husk ash (RHA) composite. *J Alloys Compd* 2017; 699: 308–322.
33. Uher C. *Thermal conductivity 25/thermal expansion 13*. Lancaster, Pennsylvania, USA: CRC Press, 2000.